

# Tunable, low-repetition-rate, cost-efficient femtosecond Ti:sapphire laser for nonlinear microscopy

P.G. Antal · R. Szipőcs

Received: 29 July 2011 / Revised version: 26 September 2011  
© Springer-Verlag 2011

**Abstract** We report on a broadly tunable, long-cavity Ti:sapphire laser oscillator being mode-locked in the net negative intracavity dispersion regime by Kerr-lens mode-locking, delivering  $\tau_{\text{FWHM}} < 300$  fs pulses at 22 MHz repetition rate. The wavelength of the laser can be tuned over a 170 nm wide range between 712 nm and 882 nm. Having a typical pump power of 2.6 W, the maximum pulse peak power is 60 kW. Comparison of the reported laser with a standard, 76 MHz Ti:sapphire oscillator regarding two-photon excitation efficiency in a laser scanning microscope shows that the 22 MHz laser generates the same fluorescence signal at considerably, 1.82 times lower average power, which is expected to result in a reduced photothermal damage probability of biological samples. This fact along with the broad tunability and a low pump power requirement makes this cost-effective laser an ideal light source for nonlinear microscopy.

## 1 Introduction

Nonlinear laser scanning microscopy is a novel 3D biomedical imaging technique with sub-micrometer resolution. There are several nonlinear optical effects that can be used for imaging, such as two- or three-photon absorption fluorescence and second-harmonic generation. To obtain the

light intensity sufficient for nonlinearities, ultrashort (fs or ps) pulse mode-locked lasers are used as light sources, most often femtosecond pulse, tunable Ti:sapphire lasers having a repetition rate at around 80 MHz.

Multiphoton transitions of intracellular fluorophores used in microscopy can be efficiently excited in the 700–1200 nm spectral region, which wavelengths penetrate deeper in tissues and are much less harmful for living specimen than direct UV illumination in single-photon fluorescent microscopy. Photochemical damage mechanisms, which can cause oxidative stress or direct DNA damage, only occur in the focus of the objective lens, where multiphoton absorption takes place. Single-photon absorption of the NIR radiation can cause photothermal damage, though this is not significant in most cells, where water is the major NIR absorber [1]. However, in cells where other efficient NIR absorbers (e.g., melanin, hemoglobin, chlorophyll) are present, photothermal damage can be a problem. Since one of the most important noninvasive diagnostic applications of nonlinear microscopy is based on *in vivo* multiphoton imaging of skin tissues [2, 3] containing a significant amount of melanin, photo-thermal damage effects should be taken care of. When the pulse repetition rate of the exciting laser radiation is not very low ( $\nu_{\text{rep}} > 5\text{--}10$  MHz), the dominating effect responsible for temperature rise and thermal damage is the cumulative heating effect of the consecutive pulses, which is proportional to the time averaged power of the pulse train incident on the sample [4]. Thus, thermal damage can be mitigated by decreasing the average power, which can be achieved by the reduction of the pulse energy or by the reduction of the repetition rate. Since two-photon absorption rate, and thus the two-photon fluorescence signal are quadratic functions of the pulse energy and linear functions of the repetition rate, mitigating thermal damage by reducing the repetition rate is preferable [4]; in [4] that was

---

P.G. Antal (✉) · R. Szipőcs  
Research Institute for Solid State Physics and Optics,  
P.O. Box 49, 1525 Budapest, Hungary  
e-mail: antal@szfki.hu  
Fax: +36-1-3922215

R. Szipőcs  
e-mail: szipoecs@sunserv.kfki.hu  
Fax: +36-1-3922215

done by using an acoustooptical pulse picker. Another way to decrease the repetition rate of a mode-locked laser is to increase the intracavity light path, i.e., the cavity length. The first long-cavity femtosecond titanium-sapphire laser was reported by Cho et al. [5]. This solution is superior to the use of a pulse picker, because every pulse is utilized for imaging, thus there is no additional power loss of the laser. Furthermore, the same pulse energy is obtained at a lower average laser power with a long-cavity oscillator than with a short-cavity one, which results in lower pump power requirement for a long-cavity laser resulting in a more cost-effective setup.

Long-cavity, low repetition rate, femtosecond, or picosecond pulse mode-locked lasers have already been used in microscopy applications, including titanium-sapphire lasers for in vivo multiphoton cytometry [6, 7]. Such titanium-sapphire oscillators as well as other extended cavity lasers with different laser materials have also been used in multifocal [8, 9] and differential [10] nonlinear microscopy. Fluorescence lifetime imaging microscopy (FLIM) also often utilizes long-cavity lasers, since some molecules with long fluorescence lifetimes can only be reliably examined with low repetition-rate pulses [11–13].

Wavelength-tunability of the light source is also important in fluorescence microscopy, since several different fluorophores are present in biological samples having different peak excitation wavelengths. This also enables wavelength selective imaging of such samples. A good example is human skin, in which different fluorescent molecules are dominant in different skin layers [2]. Wavelength-tunable femtosecond titanium-sapphire lasers operating at around 80 MHz have already been reported [14, 15], however, there are no reports on long-cavity mode-locked lasers that are wavelength-tunable.

In this paper, we report on a novel long-cavity, broadly tunable (between 712 nm and 882 nm), Kerr-lens mode-locked Ti-sapphire laser oscillator delivering nearly transform limited  $\sim 300$  fs (or shorter),  $\sim 10$  nJ pulses at 22 MHz repetition rate. The laser is solitonically mode-locked and can be operated at moderate pump power values up to 2.6 W at 532 nm, which offers the possibility of a cost-efficient laser construction. The low intracavity loss and the broad tunability range are obtained by using an ion-beam sputtered [16] ultrabroadband chirped mirror set in the laser resonator, similar to that reported in [15].

## 2 Laser setup and characterization

In order to achieve a stable, single-pulse mode-locked laser operation with soliton-like mode-locking (negative cavity dispersion), the repetition rate should not be set too low, so we decided to build a  $\sim 20$  MHz repetition rate laser. Along

with the moderate power levels used for pumping (up to 2.6 W), and  $T \sim 20\%$  transmission of the output coupler at around 800 nm, the intracavity pulse peak intensity can be kept below the multi-pulsing limit by properly setting the intracavity dispersion. We note, however, that for optimum mode-locked operation of the tunable laser at each wavelength, transmittance vs. wavelength function of the output coupler follows the gain profile of the Ti-sapphire crystal, i.e., gradually reduces for shorter and longer wavelengths as well.

To obtain the desired repetition rate, our oscillator utilizes a so called Herriott-cell (or multiple-pass cavity), which is a common feature of long-cavity laser setups [5, 17]. It consists of two spherical mirrors with multiple reflections assuring the required effective cavity length. The proper distance of the mirrors ensures that the ABCD matrix of the Herriott-cell is  $\pm$ unity, hence the long-cavity oscillator can easily be constructed by inserting this multi-pass cavity into a standard, short cavity femtosecond laser, and thus extending its cavity length, because the  $\pm$ unity matrix multi-pass cavity maintains the original mode properties of the initial resonator, optimized for Kerr-lens mode-locking. In order to attain a specific repetition rate,  $\nu_{\text{rep}}$  for a given set of Herriott-cell mirrors, the number of reflections and the distance of the mirrors are to be set according to the following formula:

$$\nu_{\text{rep}} = \frac{c}{2L_{\text{init}} + 4n \cdot L_c} = \frac{c}{2L_{\text{init}} + 8n \cdot f \cdot [1 - \cos(\frac{m}{2n}\pi)]}, \quad (1)$$

where  $c$  is the speed of light in vacuum,  $L_{\text{init}}$  is the roundtrip length of the initial resonator,  $L_c$  and  $f$  are the distance and the focal length of the Herriott-cell mirrors, respectively,  $n$  is the number of reflections on each spherical mirror and the integer  $m$  gives the total angular sweep of the beam around the optical axis of the multi-pass cavity as  $m \cdot \pi$ . With our (2" in diameter) mirrors having a 2000 mm focal length, we set up an  $n = 2$ ,  $m = 1$  ( $L_c \approx 120$  cm) Herriott-cell to build a 22 MHz long-cavity laser. The setup is shown in Fig. 1. The initial resonator, which was extended with the Herriott-cell, was a standard  $\sim 71$  MHz, astigmatically compensated resonator setup comprising a highly doped Ti:Sapphire crystal with a path length of 4 mm, pumped with a frequency doubled Nd:YVO<sub>4</sub> laser (Spectra-Physics Millennia Pro). In the long-cavity oscillator, all cavity mirrors were custom made, ion-beam sputtered ultrabroadband chirped mirrors (UBCM-s), except for the output coupler and the input coupler dichroic mirror (unfortunately, no substrate of proper thickness was available for the input coupler when the ultrabroadband mirror coating was made). The required amount of negative dispersion in the cavity is provided by an SF10 prism pair with an apex distance of 750 mm. Each prism can

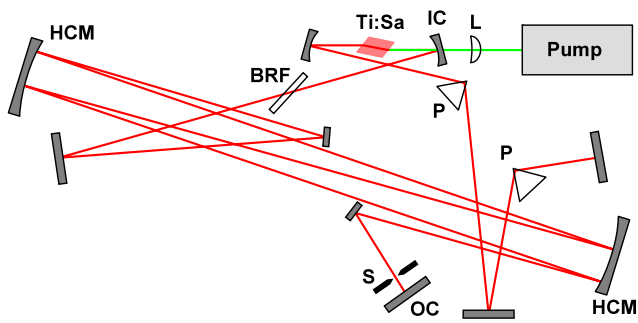


**Fig. 1** Setup of the long-cavity oscillator. L: pump focusing lens, IC: input coupler mirror, Ti:Sa: titanium-sapphire crystal BRF: birefringent filter for wavelength tuning, P: prism, HCM: Herriott-cell mirror, OC: output coupler, S: slit for hard-aperture Kerr-lens mode-locking

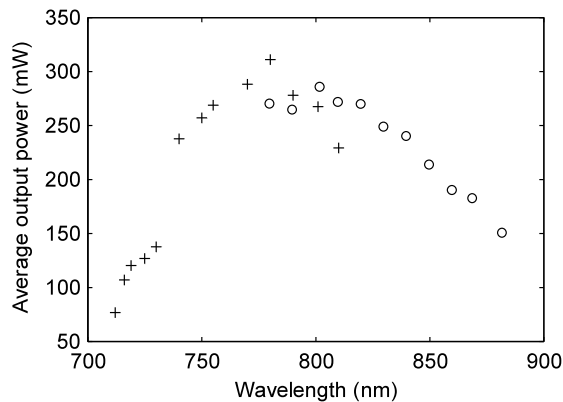


**Fig. 2** Output power versus wavelength. Two different output couplers were used for short wavelengths (SW OC, crosses) and for longer wavelengths (MW OC, circles). Pump power was between 2.29 W and 2.59 W

be translated perpendicular to its base, so the intracavity dispersion can be precisely set. The wavelength can be tuned by rotating a one-element birefringent filter (BRF) exhibiting a FWHM spectral bandwidth of  $\sim 10$  nm and a free-spectral range of  $\sim 120$  nm.

The laser can be easily mode-locked with the hard-aperture Kerr-lens mechanism by quickly translating the cavity end mirror along the optical axis, which mirror is mounted on a spring translator. The repetition rate of final laser configuration was found to be 22 MHz, as expected. The central wavelength of the laser could be tuned over a 170 nm wide range between 712 nm and 882 nm in mode-locked operation without changing cavity optics except the output coupler (“SW OC” for the 712–810 nm range and “MW OC” for the 780–882 nm range), which range is limited by the spectral width of the high reflectance band of the non-UBCM input coupler in our experimental setup. Figure 2 shows the measured average output power versus wavelength function. The pump power was properly set between 2.29 W and 2.59 W during tuning. The maximum of the measured average output power was 311 mW (at

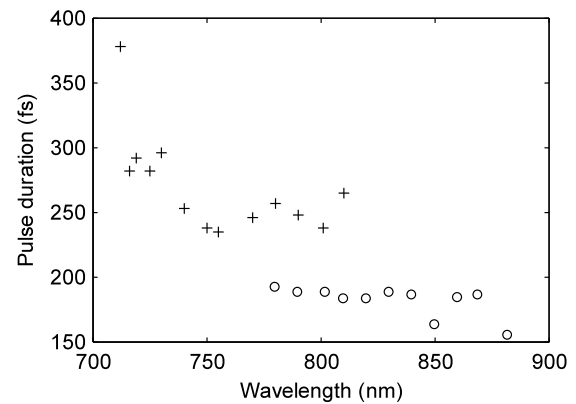


**Fig. 3** FWHM pulse duration measured during wavelength tuning. Crosses: SW OC is used; circles: MW OC is used

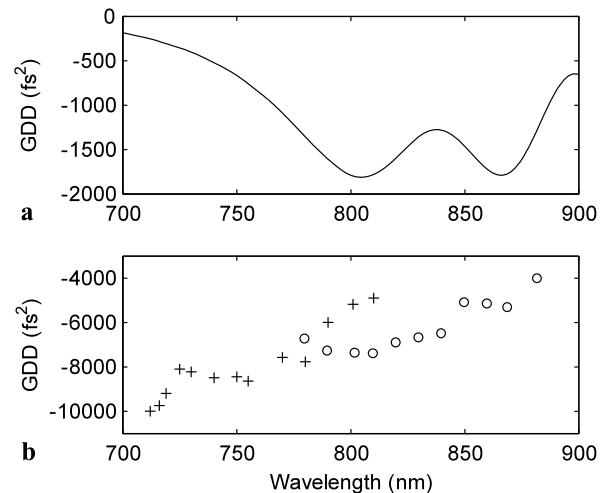


**Fig. 4** (a) Dispersion of the ultrabroadband chirped mirrors for 19 reflections. (b) Net intracavity dispersion during wavelength tuning, calculated using the dispersion curves of the UBCM-s, the calculated negative dispersion of the prism pair and the material dispersion of the laser crystal, the prism material and intracavity air. The total measurement error of the roundtrip light path length in both prisms is  $\sim 4$  mm. Crosses: SW OC is used; circles: MW OC is used

780 nm), corresponding to pulse energy of 14 nJ. The measured second-order autocorrelation trace indicates nearly transform-limited pulses with pulse duration (FWHM) of  $\sim 270$  fs when using the SW OC and  $\sim 180$  fs when using the MW OC. These measured pulse durations, depicted in Fig. 3, are determined by the intracavity dispersion (see Fig. 4b), set by precise translation of the prisms, as well as the intracavity power determined by the pump power, gain of the Ti:sapphire crystal and the intracavity loss (wavelength dependent transmittance of the output coupler) at each wavelength. Figure 4a shows the total GDD of the UBCM mirrors for one roundtrip, i.e., for 19 reflections. The GDD variation and thus the TOD of the UBCM mirrors are low enough for generation of stable, mode-locked pulses with a symmetric spectrum without considerable sidelobes (see Fig. 7). The maximum output pulse peak power during

wavelength tuning was 60 kW measured at 802 nm (when the MW output coupler was used).

### 3 Two-photon absorption fluorescence microscopy experiments

In order to demonstrate the benefits of using the 22 MHz long-cavity oscillator in multiphoton microscopy, we compared its performance to that of a standard, 76 MHz femtosecond Ti:sapphire laser of a similar optical performance (central wavelength, spectral width, beam diameter, etc.) except the repetition rate, similarly to the experiment reported in [6]. For our measurements, we used a Carl Zeiss LSM 7 MP laser scanning microscope and fluorescent microbeads (10  $\mu\text{m}$  in diameter) as samples for quantitative analysis. We excited a single fluorescent bead with each laser and measured the fluorescence signal as the function of the excitation power (measured with a semiconductor power meter, after lifting the microscope objective) in both cases. The central wavelength and the spectral width of the two lasers were adjusted and set to 800 nm and 3.7 nm, respectively, with a precision of <1 nm for the central wavelength and <0.2 nm for the spectral width. This is necessary not only for exciting the bead with the same wavelength, but also for ensuring that the laser pulses, after passing through the dispersive elements of the microscope, have practically the same duration at the sample for both lasers. (The initial chirp of the laser pulses, in case of both solitonically mode-locked lasers, is small compared to dispersion of the microscope elements, such as the acousto-optic modulator and the microscope objective.) We set the spectral width of the lasers to the above value by adjusting the intracavity dispersion and pulse energy utilizing the fact that pulse duration and spectral width depend on these parameters in lasers operating with soliton mode-locking [18] (pulse could be set by fine tuning the pump power). The FWHM beam diameter on the microscope objective entrance aperture was  $\sim 7$  mm in case of both laser sources. The excitation power could be precisely set with the built-in acousto-optic modulator of the microscope (having much larger bandwidth than the spectral width of the lasers). Power levels were varied from nearly zero fluorescence signal to saturation of the detector at a certain PMT voltage. Signal levels were determined by applying a smoothing filter on each scanned image in order to eliminate the digital noise. These evaluated values are plotted as the function of the excitation power for both lasers in Fig. 5. In principle, the two-photon excitation probability, i.e., the number of photon pairs absorbed per second ( $N$ ) is proportional to the following ratio [4]:

$$N \propto \frac{E^2 \nu_{\text{rep}} \delta}{A^2 \tau} = \frac{1}{\nu_{\text{rep}}} \frac{\delta}{A^2 \tau} \cdot P_{\text{av}}^2 \quad (2)$$

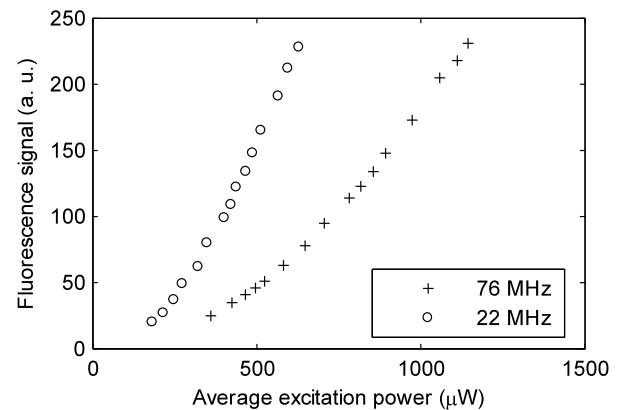


**Fig. 5** Two-photon absorption fluorescence signal of a microbead as the function of NIR (800 nm) excitation power, using the 76 MHz laser (crosses) and then the 22 MHz laser (circles) as light sources

where  $E$  is the pulse energy,  $\nu_{\text{rep}}$  is the repetition rate,  $\delta$  is the two-photon absorption cross-section,  $\tau$  is the pulse duration,  $A$  is the effective mode area (spot size) of the beam in the focus, and  $P_{\text{av}}$  is the average excitation power. According to (2), we fitted a parabola ( $y = C \cdot x^2$ ) on each of the measured curves in Fig. 5. From this procedure, we obtained 3.33 times higher  $C$  value for the 22 MHz laser than for the 76 MHz laser. This means that  $3.33^{1/2} = 1.82$  times lower average power is needed for generating the same fluorescence signal with the 22 MHz oscillator than with the 76 MHz one. Thus we expect that the thermal damage probability is reduced when the 22 MHz laser is used instead of the 76 MHz laser. The extent of this reduction depends on the absorption coefficients of the material components in the sample and the pulse energy. From (2), the ratio of the  $C$  constants is expected to be the inverse of the ratio of the repetition rates, provided that all of the other parameters ( $A$ ,  $\tau$  and  $\delta$ ) are the same. This ratio is 3.45 in our case. We can say that the measured two-photon fluorescence signal ratio agrees well with the theoretical value. The slight deviation can be attributed to the fact that the mode profiles were slightly different for the two lasers (the 76 MHz laser beam had some slight ellipticity) at the entrance aperture of the microscope, resulting in somewhat different spot sizes in the focus.

Comparison of the two lasers was also performed using a biological sample, a piece of un-haired dorsal skin of a mouse. In Fig. 6, the two-photon absorption images of the surface of the skin is shown, where fluorescence originates mainly from keratin. The two images were taken at nearly the same excitation power. It is apparent from the intensity profiles (recorded along the white horizontal line in the middle of the images) that the fluorescence signal is again approximately 3.3 times higher when using the long-cavity laser as a light source.

Pulse durations at the long cavity laser's output and at the focus of the microscope objective were also determined.

**Fig. 6** Two-photon absorption fluorescence raw images of mouse dorsal skin using (a) the 76 MHz laser and (b) the 22 MHz laser, at nearly the same excitation power (3.081 mW for the 76 MHz laser and 3.015 mW for the 22 MHz laser). (c) and (d) show the corresponding intensity profiles along the white horizontal line in the middle of the images

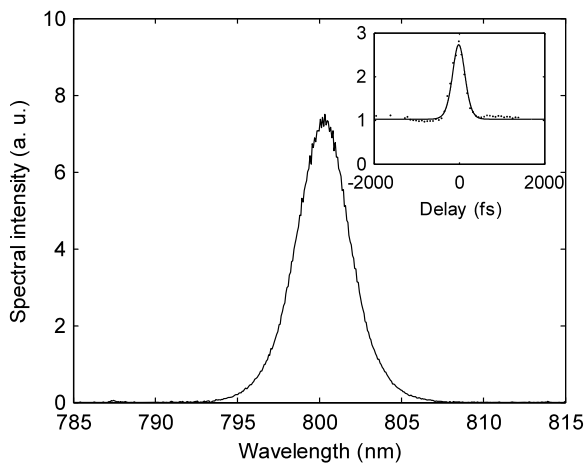
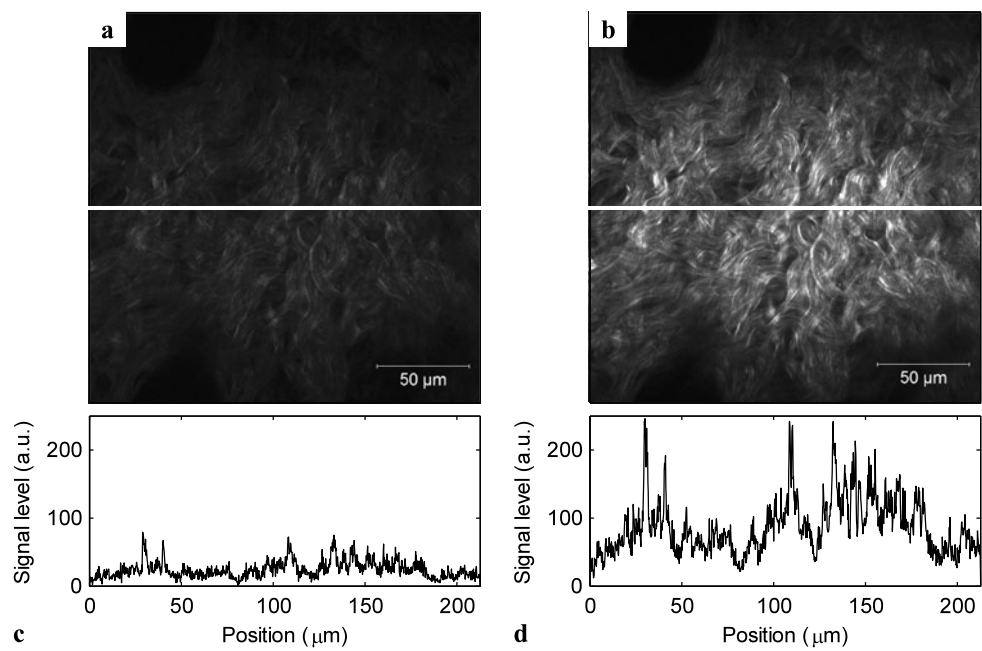


**Fig. 7** Spectrum of the 22 MHz laser. The corresponding second-order autocorrelation trace measured at the focus of the microscope objective is in the inset graph (the vertical axis is the normalized second order autocorrelation signal). Measured data points: dots, fitted curve: solid line. The full width at half maximum of the fitted curve is 342 fs, which corresponds to a FWHM pulse duration of approximately 221 fs in the focus

From the second-order autocorrelation measurement, we obtained a FWHM pulse duration of  $190 \pm 5$  fs at the output of both lasers (for  $\text{sech}^2$  pulse shape). Figure 7 shows the corresponding,  $\text{sech}^2$  shaped spectrum, having an FWHM bandwidth of 3.76 nm. At the focus of the objective lens, the second-order autocorrelation trace could be measured by recording the two-photon absorption fluorescence signal [19] of the microbeads as the function of delay set in a Michelson interferometer placed between the long-cavity laser and the laser scanning microscope. For technical rea-

sons, we measured the second-order interferometric autocorrelation by recording sections of three neighboring oscillation periods, the sections being 70 fs apart from each other, and averaging over each section. The result is shown in the inset of Fig. 7. From fitting of the theoretical formula for the autocorrelation of  $\text{sech}^2$  pulses, the pulse duration in the focus is estimated to be around 221 fs.

#### 4 Conclusions

A wavelength-tunable, long-cavity, low-repetition-rate (22 MHz) laser is demonstrated. The tuning range is 170 nm wide which enables several different fluorescent molecules present in biological samples to be excited with this light source. Owing to the low repetition rate, the laser is a promising candidate for nonlinear microscopy, as far as photothermal damage mechanisms and price of the laser are concerned. As for in vivo microscopy applications of our novel laser, however, further detailed investigations have to be done in the future, regarding photochemical degradation of living cells, especially DNA damage [20] due to multiphoton absorption. Fluorescence lifetime measurement or fluorescence lifetime imaging microscopy could be another possible application of this laser oscillator for samples that contain fluorophores having fluorescence lifetime up to 15 ns, assuming that the time period between successive laser pulses should be at least three times longer than the longest component of the fluorescence decay under investigation [11, 12].

**Acknowledgements** We gratefully acknowledge the fruitful discussions with Attila Kolonics on biological issues related to nonlinear microscopy. We also thank Attila Szigligeti and Dóra Haluszka for their technical assistance. This research was supported by the Hungarian Development Agency (NFÜ) under contract no. TECH-09-A2-2009-0134 and by R&D Ultrafast Lasers Ltd. under contract no. BAROSS-KM07-KM-TERM-07-2008-0003.

**Note added in proof** By further optimizing the adjustable resonator parameters (distance between the laser crystal and the pump input coupler mirror and the distance between this mirror and the other concave mirror behind the crystal), we managed to improve the Kerr-lens mode-locking stability and thus extend the width of the tuning range of the 22 MHz laser to 185 nm (the wavelength range between 700 nm and 885 nm).

## References

1. K. König, T.W. Becker, P. Fischer, I. Riemann, K.-J. Halhuber, *Opt. Lett.* **24**, 113 (1999)
2. H.G. Breunig, H. Studier, K. König, *Opt. Express* **18**, 7857 (2010)
3. K. König, *Proc. SPIE* **7883**, 78830D (2011)
4. B.R. Masters, P.T.C. So, C. Buehler, N. Barry, J.D. Sutin, W.W. Mantulin, E. Gratton, *J. Biomed. Opt.* **9**, 1265 (2004)
5. S.H. Cho, B.E. Bouma, E.P. Ippen, J.G. Fujimoto, *Opt. Lett.* **24**, 417 (1999)
6. E.R. Tkaczyk, J.Y. Ye, S. Katnik, K. Luker, G. Luker, J.R. Baker, in *Conference on Lasers and Electro-Optics/Quantum Electronics and Laser Science Conference and Photonic Applications Systems Technologies*. OSA Technical Digest Series (CD) (Optical Society of America, Washington, 2007), paper CTuP7
7. E.R. Tkaczyk, C.F. Zhong, J.Y. Ye, S. Katnik, A. Myc, T. Thomas, K.E. Luker, G.D. Luker, J.R. Baker, in *Novel Optical Instrumentation for Biomedical Applications III*, ed. by C. Depeursinge. Proceedings of SPIE-OSA Biomedical Optics, vol. 6631 (Optical Society of America, Washington, 2007), paper 6631\_31
8. R. Carriles, K.E. Sheetz, E.E. Hoover, J.A. Squier, V. Barzda, *Opt. Express* **16**, 10364 (2008)
9. K.E. Sheetz, E.E. Hoover, R. Carriles, D. Kleinfeld, J.A. Squier, *Opt. Express* **16**, 17574 (2008)
10. D. Sandkuijl, R. Cisek, A. Major, V. Barzda, *Biomed. Opt. Express* **1**, 895 (2010)
11. S. Lévêque-Fort, D.N. Papadopoulos, S. Forget, F. Balembois, P. Georges, *Opt. Lett.* **30**, 168 (2005)
12. A. Major, V. Barzda, P.A.E. Piunno, S. Musikhin, U.J. Krull, *Opt. Express* **14**, 5285 (2006)
13. P. Blandin, F. Druon, M. Hanna, S. Lévêque-Fort, C. Lesvigne, V. Couderc, P. Leproux, A. Tonello, P. Georges, *Opt. Express* **16**, 18844 (2008)
14. J.D. Kafka, M.L. Watts, J.-W.J. Pieterse, *IEEE J. Quantum Electron.* **28**, 2151 (1992)
15. E.J. Mayer, J. Möbius, A. Euteneuer, W.W. Rühle, R. Szipőcs, *Opt. Lett.* **22**, 528 (1997)
16. B. Császár, A. Kőházi-Kis, R. Szipőcs, in *Conference on Lasers and Electro-Optics/Quantum Electronics and Laser Science and Photonic Applications Systems Technologies*, Baltimore, Maryland, USA, 2005. Technical Digest (CD) (Optical Society of America, Washington, 2005), paper JWB15
17. D. Herriott, H. Kogelnik, R. Kompfner, *Appl. Opt.* **3**, 523 (1964)
18. F. Krausz, M.E. Fermann, T. Brabec, P.F. Curley, M. Hofer, M.H. Ober, C. Spielmann, E. Wintner, A.J. Schmidt, *IEEE J. Quantum Electron.* **28**, 2097 (1992)
19. M. Müller, J. Squier, G.J. Brakenhoff, *Opt. Lett.* **20**, 1038 (1995)
20. F. Fischer, B. Volkmer, S. Puschmann, R. Greinert, W. Breitbart, J. Kiefer, R. Wepf, *Proc. SPIE* **6191**, 619105 (2006)